Controlling Pattern Formation in Nanoparticle Assemblies via Directed Solvent Dewetting

Christopher P. Martin, Matthew O. Blunt, Emmanuelle Pauliac-Vaujour, Andrew Stannard, and Philip Moriarty*
School of Physics and Astronomy, The University of Nottingham, University Park, Nottingham NG7 2RD, United Kingdom

Ioan Vancea and Uwe Thiele
Max Planck Institute for the Physics of Complex Systems, Nöthnitzer Strasse 38, D-01187 Dresden, Germany
(Dated: July 11, 2007)

We have achieved highly localised control of pattern formation in two dimensional nanoparticle assemblies by direct modification of solvent dewetting dynamics. A striking dependence of nanoparticle organisation on the size of atomic force microscope-generated surface heterogeneities is observed and reproduced in numerical simulations. Nanoscale features induce rupture of the solvent-nanoparticle film, causing the local flow of solvent to carry nanoparticles into confinement. Microscale heterogeneities instead slow the evaporation of the solvent, producing a remarkably abrupt interface between different nanoparticle patterns.

PACS numbers: 68.05.Cf, 68.08.Bc, 61.46.Df

Colloidal solutions of nanoparticles are simple to synthesise, exceptionally stable, and can be made from materials with a wide variety of chemical and electrical properties. Their versatility makes them ideal building blocks for the next generation of nanoscale electronic devices. When deposited on a surface, colloidal nanoparticles form a diverse array of patterns[1–8] for which the behaviour of the solvent plays a key role. Isolated islands, worm-like domains, continuous labyrinthine patterns, and polygonal networks can each be produced by varying the experimental conditions [1, 5, 9, 10]. Although there have been impressive recent examples of the exploitation of dewetting to form stripes of nanoparticles[6, 7, 11], spatial control of dewetting-induced pattern formation in 2D assemblies of nanoparticles has to date not been demonstrated.

Here we describe highly localised control of 2D pattern formation in colloidal nanoparticle arrays via surface inhomogeneities created by atomic force microscope (AFM)-induced oxidation. In addition to representing a new technique for nanostructure control, our experiments and associated simulations provide key insights into the mechanisms of surface inhomogeneity-directed self-organisation in nanoparticle systems. Whereas nanoscale surface features drive the rupture of the solvent-nanoparticle film, microscale oxide features on an otherwise hydrophobic surface retard solvent evaporation, providing important complementary stategies for spatial control of dewetting dynamics. We also show that a simple modification of the Hamiltonian introduced by Rabani et al.[9], can reproduce important experimentally observed patterns not captured by the original code.

Our experiments are based on AFM-induced oxidation of hydrogen-passivated Si(111) surfaces[12, 13]. An Asylum Research MFP-3D AFM system operating in intermittent contact mode with closed-loop control was used for both imaging and local oxidation of the H:Si(111) samples. Oxidation was carried out using PtIr-coated silicon probes at a bias of -10V, and in 70% humidity. Octanethiol-passivated Au nanoparticles were prepared in toluene[14]. For experiments involving rapid solvent evaporation, a 25μl droplet of an appropriately diluted solution was placed on the locally oxidised substrate and the sample subsequently spun at 4krpm. Slow evaporation was induced by keeping the solvent in a meniscus on the sample by means of a small PTFE ring.

The 2D Ising model simulations described by Rabani et al. [9] are capable of replicating a large number of the nanoparticle structures seen in experiment. In particular, certain classes of cellular structure are reproduced with an accuracy that renders them statistically indistinguishable from experiment [10, 15]. There are, however, a number of common experimental phenomena that cannot be simulated by this method, and which are of key importance to our studies of directed dewetting. For example, Fig. 1(a) shows a structure that is frequently observed in our experiments. A Fourier transform[16] reveals that the pattern exhibits not just one, but two preferred cell sizes, each having a relatively wide distribution. The nature of the structures produced by the simulation is governed by the parameters in the Hamiltonian

$$E = -\epsilon_l \sum_{<ij>} l_i l_j - \epsilon_n \sum_{<ij>} n_i n_j - \epsilon_{nl} \sum_{<ij>} n_i l_j - \mu \sum_i l_i, \quad (1)$$

where ϵ_l, ϵ_n, and ϵ_{nl} are the liquid-liquid, nanoparticle-nanoparticle, and nanoparticle-liquid interaction energies respectively. As discussed by Rabani et al. [9], the value of μ (the chemical potential) determines the mean equilibrium density of solvent, and is an effective parameter representing any interaction energy that is not explicitly

taken into account by the other parameters.

Although the original model was two-dimensional, Yosef and Rabani[17] have recently extended it to three dimensions. To take into account the 3D nature of the solvent film, we have adopted a rather different approach which involves a simple change to the Hamiltonian of the original 2D model. By making the chemical potential an explicit function of the global solvent density, we can model an increase in μ as the solvent layer thins during evaporation. This density dependence corresponds to a thickness- dependent disjoining pressure[18] accounting for substrate wettability in continuum models [19, 20]. As a result, the solvent evaporates with a rate inversely proportional to its coverage (Fig. 1). Fig. 1(b) shows the result of this modification, which matches the experimental image not just qualitatively, but also quantitatively[15, 16]. Increasing the coupling between μ and solvent coverage (Fig. 1(d)) replicates the effect of using chloroform in the experiments (Fig. 1(c)). Importantly, the nanoparticle rings [17, 21, 22] in these simulated structures are formed spontaneously, without the manual introduction of nucleation sites described by Yosef and Rabani [17] - a technique discussed below.

The behaviour of the solvent plays a critical role in determining the nature of the nanoparticle patterns; to a large extent, the particles are merely passengers on the tide of the solvent, and their final positions describe the history of flow and evaporation. Modifying the surface of the substrate to perturb the behaviour of the solvent must therefore lead to a modification of the nanoparticle structures.

Fig. 2(a) shows the striking effect on nanoparticle organisation of an AFM-oxidised $4 \times 4\mu m^2$ square on H:Si(111)[12, 13]. There is an extremely sharp transition from a cellular structure on the oxide to a broken worm-like pattern elsewhere. Given that the edge of the oxide region should in principle represent a steep gradient in wettability, with strong implications for dewetting-mediated pattern formation[23, 24], the lack of a region denuded of nanoparticles at the edge of the oxide is intriguing. We return to a discussion of this important point below. Simulations indicate that cellular networks are generated by slower solvent evaporation than that which occurs in the formation of labyrinthine structures [9, 15]. This would suggest that evaporation is somehow

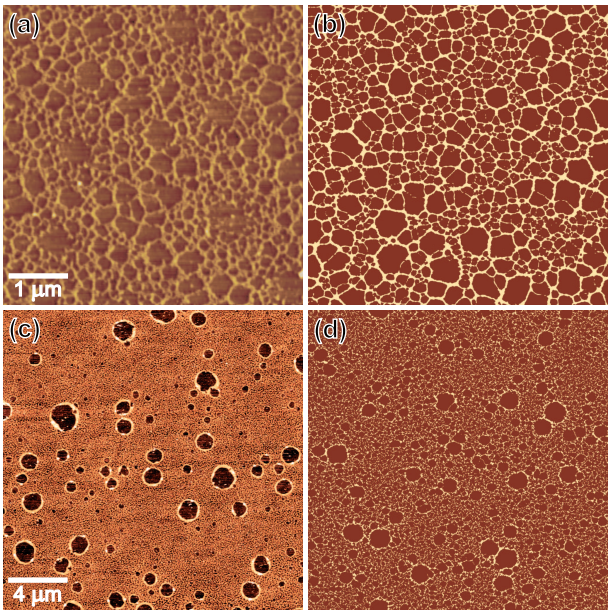

FIG. 1: (a) An AFM image of a two-level cellular structure formed by spin-casting gold nanoparticles in toluene onto a silicon substrate, (b) a simulated structure formed by linking the chemical potential (μ) to the solvent density (in the form $\mu(v) = \mu_0 + (0.1\mu_0 \times v^{0.7})$, where v is the fraction of solvent that has become vapour, and μ_0 is the value of μ at the beginning of the simulation), (c) an AFM image of gold nanoparticles spun onto silicon from chloroform, and (d) a simulated image with a much stronger coupling between μ and solvent coverage (in the form $\mu(v) = \mu_0 + (0.5\mu_0 \times v^{0.7})$).

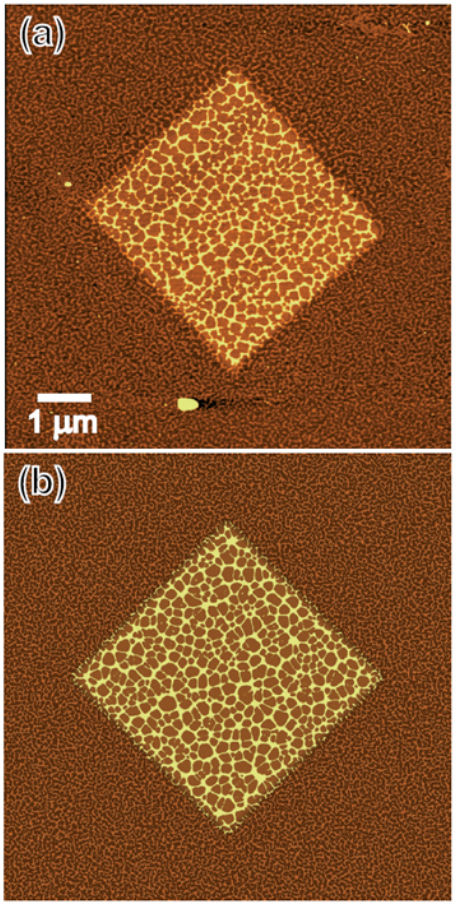

FIG. 2: (a) An AFM image of gold nanoparticles spun from toluene onto H:Si(111) with an AFM-patterned $4\mu m \times 4\mu m$ square of oxide in the centre, and (b) the result of a simulation with $|\mu|$ 6% lower on the oxide area.

retarded by the presence of the oxide, i.e. the solvent

finds the oxide areas more wettable. Fig. 2(b) shows the result of spatially varying the value of μ, such that its modulus is very slightly (6%) lower on the oxide than in the surrounding area, with an interface region comprising a 100nm linear transition. This equates to a greater wettability in the region of the oxide. The image shown in Fig. 2(b) matches the experimental result extremely well.

Contact angle measurements show, however, that there is no observable difference in the wettability of macroscopic volumes of toluene on H:Si(111) and native oxide-terminated Si(111) surfaces having comparable roughness. Both substrates yield a contact angle close to zero ($\approx 5°$), albeit with a very large error bar ($\pm 50\%$). These measurements would seem to be at odds not only with the results of Fig. 2, where a greater wettability of the oxide region is observed, but with estimates of Hamaker constants [18] which yield different signs for the air/toluene/silicon and air/toluene/silicon oxide systems. We can, however, explain these apparent discrepancies between wetting theory and experiment in terms of the nanoscale structure of the SiO-Si system. First, as pointed out by Seeman et al. [25], the appropriate system to consider for the estimation of Hamaker constants is air/toluene/SiO/Si where the native oxide layer is $\approx$2 nm thick. In this context, the high wettability of toluene on native oxide-terminated silicon seen in the contact angle measurements is not unexpected. Second, and of key importance for our directed dewetting experiments, the stronger affinity of the apolar solvent for the oxide region rather than for the H:Si(111) surface in Fig. 2 can largely be rationalised in terms of the higher degree of roughness/porosity of silicon oxide formed using scanning probe nanolithography as compared to oxides prepared by more conventional methods [26, 27].

Below a critical feature linewidth ($\approx$200nm), the effect of oxide regions on the far-from-equilibrium flow of solvent is radically different from that shown in Fig. 2. Fig. 3(a) shows nanoparticle patterns formed in the presence of SiO_2 rings of 1μm diameter on H:Si(111). The 100nm-wide lines are almost completely free of particles, and a clearly denuded zone extends around them for a further 100nm. It is possible to reproduce this effect in our simulations by completely removing sections of solvent and nanoparticles from regions representing the oxide rings prior to the start of the simulation. This is similar to the technique employed by Yosef and Rabani [17].

The importance of dewetting nucleated by a gradient in wettability has been discussed in some depth for thin polymer films on heterogeneous substrates [23, 24].

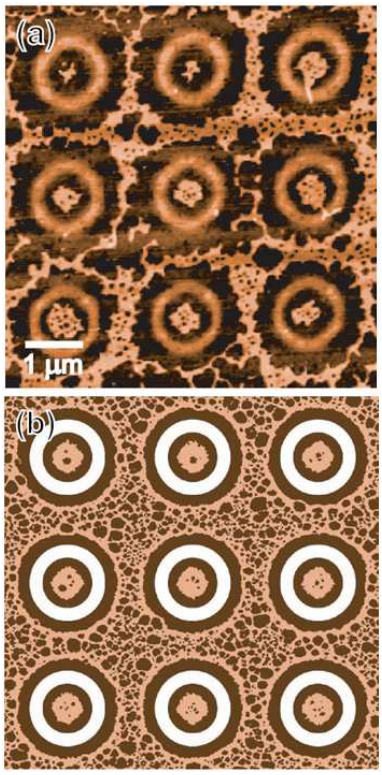

FIG. 3: (a) An AFM image showing the effect of 1μm diameter rings of oxide on nanoparticle pattern formation, and (b) a simulation in which sections of solvent and particles have been removed (indicated in white) to approximate the effect of dewetting from the oxide regions before the realm of the simulation.

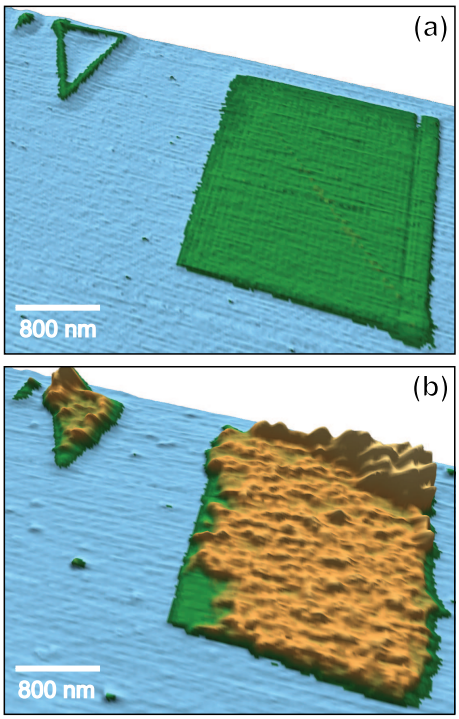

FIG. 4: (a) A three-dimensional rendering of an AFM image of raised oxide areas on H:Si(111), and (b) the same areas covered with trapped nanoparticles after slow evaporation of a gold nanoparticle solution.

While a wettability gradient exists for the AFM-defined patterns shown in both Fig. 2 and Fig. 3, it is only for the latter that a denuded zone free of nanoparticles is observed in the vicinity of the surface heterogeneity, indicating that the feature linewidth plays a fundamental role in driving the rupture of the solvent/nanoparticle film[16]. In addition to the chemical heterogeneity represented by the oxide regions, as the solvent thins by evaporation, there comes a point when the 3nm height difference of the small oxide regions becomes very significant. These regions are likely to be the first in which the thickness of the film becomes small enough for the disjoining pressure to cause nucleation of a hole in the film. This tailor-made hole will then grow by evaporation, isolating a small group of nanoparticles inside the ring. A simulation including this modification, and also a solvent density-dependent chemical potential (see Fig. 1), is shown in Fig. 3(b). This directed dewetting process enables confinement within specific nanoscale surface regions *without the need for chemical functionalisation of the nanoparticles*.

The effect of the greater roughness of the oxide regions can be exploited in an experimental regime that is much closer to equilibrium conditions. The oxide square in Fig. 4(a) has more than twice the RMS roughness of the surrounding H:Si(111) surface. When a nanoparticle solution is allowed to evaporate from this surface over a period of hours rather than seconds, the significantly decreased mobility of the particles on the rougher areas becomes apparent. This slow evaporation mode proceeds by a gradual horizontal "retreat" of the solvent as it evaporates. Particles that are otherwise quite mobile tend to accumulate on the roughened areas as the solvent retreats over them. Unable to escape, they build up to form a near complete single layer that is confined within the boundary of the oxide (Fig. 4(b)). Moreover, we find that a triangular "box" with boundaries just a few tens of nm wide has a similar effect. A close-packed monolayer is formed as particles enter the container from solution, only to find themselves unable to surmount the walls and follow the solvent as the thinning edge withdraws.

The ability to control pattern formation by locally directing solvent dewetting is an important development on the road to self-organised nanoparticle devices. A lack of requirement for particle functionalisation allows this technique to be employed with a wide range of different particle types. The approach we describe thus opens up a rich new parameter space in directing the assembly of nanoparticle arrays.

We are grateful for the financial support of the U.K. EPSRC and the EU Framework Programme 6 Marie Curie scheme (under grant MRTN-CT-2004005728 (PATTERNS)). We also would like to very gratefully acknowledge helpful discussions with James Sharp, Ulli Steiner, and Coen van den Brom.

* Electronic address: philip.moriarty@nottingham.ac.uk

[1] G. Ge and L. Brus, J. Phys. Chem. B **104**, 9573 (2000).
[2] P. Moriarty, M. D. R. Taylor, and M. Brust, Phys. Rev. Lett. **89**, 248303 (2002).
[3] S. Narayanan, J. Wang, and X.-M. Lin, Phys. Rev. Lett. **93**, 135503 (2004).
[4] T. P. Bigioni, X.-M. Lin, T. T. Nguyen, E. I. Corwin, T. A. Witten, and H. M. Jaeger, Nature Mat. **5**, 265 (2006).
[5] M. O. Blunt, C. P. Martin, M. Ahola-Tuomi, E. Pauliac-Vaujour, P. Sharp, P. Nativo, M. Brust, and P. J. Moriarty, Nature Nanotech. **2**, 167 (2007).
[6] J. Huang, F. Kim, A. R. Tao, S. Connor, and P. Yang, Nature Mat. **4**, 896 (2005).
[7] N. Lu, X. Chen, D. Molenda, A. Naber, H. Fuchs, D. V. Talapin, H. Weller, J. Mller, J. M. Lupton, J. Feldmann, et al., Nano Lett. **4**, 885 (2004).
[8] A. J. Parker, P. A. Childs, R. E. Palmer, and M. Brust, Nanotechnology **12**, 6 (2001).
[9] E. Rabani, D. R. Reichman, P. L. Geissler, and L. E. Brus, Nature **426**, 271 (2003).
[10] C. Martin, M. O. Blunt, E. Pauliac-Vaujour, A. Fahmi, A. D'Aleo, L. D. Cola, and F. Vogtle, *Systems Self-assembly: Interdisciplinary Snapshots* (eds. N. Krasnogor, S. Gustafson, D. Pelta, and J. L. Verdegay, Elsevier, at press, 2007).
[11] J. Xu, J. Xia, and Z. Lin, Angew. Chem. Int. Ed. **46**, 1860 (2007).
[12] P. Avouris, R. Martel, T. Hertel, and R. Sandstrom, Appl. Phys. A **66**, S659 (1998).
[13] J. A. Dagata, Science **8**, 1625 (1995).
[14] M. Brust, M. Walker, D. Bethell, D. J. Schiffrin, and R. Whyman, J. Chem. Soc., Chem. Commun. **7**, 801 (1994).
[15] C. P. Martin, M. O. Blunt, and P. Moriarty, Nano Letters **4**, 2389 (2003).
[16] C. P. Martin, M. O. Blunt, E. Pauliac-Vaujour, A. Stannard, P. Moriarty, I. Vancea, and U. Thiele, Supplementary material for this paper, EPAPS 0000 (2007).
[17] G. Yosef and E. Rabani, J. Phys. Chem. B **110**, 20965 (2006).
[18] J. N. Israelachvili, *Intermolecular and Surface Forces* (Academic Press, 1992), 2nd ed.
[19] P. G. de Gennes, Rev. Mod. Phys. **57**, 827 (1985).
[20] U. Thiele, Eur. Phys. J. E **12**, 409 (2003).
[21] P. C. Ohara and W. M. Gelbart, Langmuir **14**, 3418 (1998).
[22] M. Maillard, L. Motte, and M. P. Pileni, Adv. Mater. **13**, 200 (2001).
[23] R. Konnur, K. Kargupta, and A. Sharma, Phys. Rev. Lett. **84**, 931 (2000).
[24] L. Brusch, H. Kühne, U. Thiele, and M. Bär, Phys. Rev. E **66**, 011602 (2002).
[25] R. Seemann, S. Herminghaus, and K. Jacobs, Phys. Rev. Lett. **86**, 5534 (2001).
[26] P. Avouris, T. Hertel, and R. Martel, Appl. Phys. Lett. **71**, 285 (1997).
[27] J. Bico, U. Thiele, and D. Quéré, Colloids and Surfaces A: Physicochem. Eng. Aspects **206**, 41 (2002).